Published in final edited form as:

Nature. 2015 December 24; 528(7583): 565–569. doi:10.1038/nature16451.

Unique role for ATG5 in PMN-mediated immunopathology during *M. tuberculosis* infection

Jacqueline M. Kimmey[1], **Jeremy P. Huynh**[1], **Leslie A. Weiss**[1], **Sunmin Park**[2], **Amal Kambal**[2], **Jayanta Debnath**[3], **Herbert W. Virgin**[2], and **Christina L. Stallings**[1,#]

[1]Department of Molecular Microbiology, Washington University School of Medicine, St Louis, MO, USA

[2]Department of Pathology and Immunology, Washington University School of Medicine, St. Louis, MO, USA

[3]Department of Pathology and Helen Diller Family Comprehensive Cancer Center, University of California, San Francisco, San Francisco, California, USA

Summary Paragraph

Mycobacterium tuberculosis (*Mtb*), a major global health threat, replicates in macrophages (MΦ) in part by inhibiting phagosome-lysosome fusion, until IFN-γ activates the MΦ to traffic *Mtb* to the lysosome. How IFN-γ elicits this effect is unknown, but many studies suggest a role for macroautophagy (autophagy herein), a cellular process by which cytoplasmic contents are sequestered into an autophagosome and targeted for lysosomal degradation[1]. The involvement of autophagy has been defined based on studies in cultured MΦ or dendritic cells (DC) where *Mtb* colocalizes with autophagy (ATG) factors ATG5, ATG12, ATG16L1, p62, NDP52, Beclin1 and LC3[2–6], stimulation of autophagy increases bacterial killing[6–8], and inhibition of autophagy allows for increased bacterial survival[1,2,4,6,7]. Notably, these studies reveal modest (e.g. 1.5- to 3-fold change) effects on *Mtb* replication. In contrast, *Atg5*$^{fl/fl}$*-LysM-Cre* mice lacking ATG5 in monocyte-derived cells and neutrophils (polymorphic mononuclear cells, PMN) succumb to *Mtb* within 30 days[4,9], an extremely severe phenotype similar to mice lacking IFN-γ signaling[10,11]. Importantly, ATG5 is the only ATG factor that has been studied during *Mtb* infection *in vivo* and autophagy-independent functions of ATG5 have been described[12–18]. For this reason, we used a genetic approach to elucidate the role for multiple ATG genes and the requirement for autophagy in resistance to *Mtb* infection *in vivo*. We have discovered that, contrary to expectation, autophagic capacity does not correlate with the outcome of *Mtb* infection. Instead, ATG5 plays a unique role in protection against *Mtb* by preventing PMN-mediated immunopathology. Furthermore, while

#Correspondence to: Christina L. Stallings, Department of Molecular Microbiology, Washington University School of Medicine, Box 8230, 660 South Euclid Avenue, Saint Louis Missouri 63110, Phone: 314-286-0276, ; Email: stallings@wusm.wustl.edu

Supplemental Information is linked to the online version of the paper at www.nature.com/nature

Author Contributions. J.M.K. designed and performed experiments, analyzed data, and wrote the manuscript. J.P.H. and L.A.W. performed experiments. S.P., A.K., and J.D. generated mouse strains. H.W.V. provided all mouse strains, analyzed data and wrote the manuscript. C.L.S. designed experiments, analyzed data and wrote the manuscript.

The authors have no competing financial interests to declare.

ATG5 is dispensable in alveolar MΦ during *Mtb* infection, loss of *Atg5* in PMN can sensitize mice to *Mtb*. These findings shift our understanding of the role of ATG5 during *Mtb* infection, reveal a new outcome of ATG5 activity, and shed light on early events in innate immunity that are required to regulate tuberculosis disease pathology and *Mtb* replication.

Main Text

We first replicated the finding that *Atg5* is critical in myeloid-derived cells for resistance to *Mtb* by infecting *Atg5*$^{fl/fl}$*-LysM-Cre* mice[4,9]. LysM-promoter-driven expression of Cre recombinase (*LysM-Cre*) results in deletion of a floxed gene in alveolar MΦ, recruited MΦ, inflammatory monocytes, monocyte-derived DC, and PMN[19,20]. Following aerosol inoculation of *Mtb* into wild-type C57Bl/6 mice, bacteria replicate in innate immune cells until IFN-γ producing T cells are recruited to the lungs between 18 – 20 days post infection (dpi), resulting in control of bacterial burden and survival[21]. Consistent with previous publications[4,9], *Atg5*$^{fl/fl}$*-LysM-Cre* mice lost 23% of their weight by 20 dpi and succumbed to *Mtb* between 30 – 40 dpi (Fig. 1a, b). In contrast, *Atg5*$^{fl/fl}$ control mice showed no signs of sickness or weight loss. Bacterial titers in *Atg5*$^{fl/fl}$*-LysM-Cre* mice were significantly higher at 3 weeks post infection (wpi) than those in *Atg5*$^{fl/fl}$ mice (Fig. 1c, d). By 5 wpi, *Atg5*$^{fl/fl}$ mice had controlled pulmonary burden while *Atg5*$^{fl/fl}$*-LysM-Cre* mice rapidly succumbed to infection (Fig. 1b, c).

In cultured cells, *Atg5*, *p62*/SQSTM1, and *Ulk1* have similar roles in controlling *Mtb* survival and replication[1,4,5,22]. We therefore explored the role of these and other genes involved in autophagy *in vivo*, by infecting mice with germline deletions of *Ulk1*, *Ulk2* (autophagy induction), *Atg4B* (isolation membrane elongation), or *p62*/SQSTM1 (substrate targeting to autophagosome). Surprisingly, mice lacking *Ulk1, Ulk2, Atg4B* or *p62* showed no signs of sickness during infection, efficiently controlled bacterial burden, and survived over 80 days with *Mtb* (Fig. 1e–h, and Extended Data Fig. 1a). Potential redundancy may explain the lack of a phenotype in *Ulk1*$^{-/-}$, *Ulk2*$^{-/-}$, *Atg4B*$^{-/-}$, and *p62*$^{-/-}$ mice during *Mtb* infection. However, loss of either *Ulk1* or *Ulk2* results in clear autophagy defects in cultured cells[23], and *Atg4B*$^{-/-}$ mice have dramatic autophagy defects in many tissues, including a nearly complete loss of LC3-II formation in the lungs, kidney and liver[24]. Regardless of issues with redundancy, these data indicate a lack of correlation between *in vitro* and *in vivo* findings of the roles of these genes in controlling *Mtb* replication.

We next tested the role of essential ATG genes other than *Atg5* in resistance to *Mtb*. If ATG5 is required *in vivo* due to its role in canonical autophagy, then *LysM-Cre* deletion of other essential autophagy genes would result in a similar phenotype as observed in *Atg5*$^{fl/fl}$*-LysM-Cre* mice. Contrary to expectation, *Atg14L*$^{fl/fl}$*-LysM-Cre*, *Atg12*$^{fl/fl}$*-LysM-Cre*, *Atg16L1*$^{fl/fl}$*-LysM-Cre*, *Atg7*$^{fl/fl}$*-LysM-Cre* and *Atg3*$^{fl/fl}$*-LysM-Cre* mice did not show any signs of sickness or weight loss following infection with *Mtb* and all survived over 80 dpi (Fig. 1i and Extended Data Fig. 1b). In addition, these mice were all able to control *Mtb* burden in a manner similar to C57Bl/6 mice (Fig. 1j, k). These findings were particularly notable as these same *Atg16L1*$^{fl/fl}$*-LysM-Cre*, *Atg7*$^{fl/fl}$*-LysM-Cre* and *Atg3*$^{fl/fl}$*-LysM-Cre* mice are dramatically more susceptible to *Toxoplasma gondii*, another pathogen for which IFN-γ

plays a key role in resistance to infection[12,14]. Nevertheless, to compare the relative efficacy of conditional deletion of each essential autophagy factor, LC3 lipidation and p62 degradation were measured *ex vivo* in peritoneal exudate MΦ (Fig. 1l) and bronchoalveolar lavage MΦ (Extended Data Fig. 2). Consistent with previous publications utilizing these mouse strains[12,14], the floxed alleles in *Atg5$^{fl/fl}$-LysM-Cre*, *Atg16L1$^{fl/fl}$-LysM-Cre*, *Atg7$^{fl/fl}$-LysM-Cre* and *Atg3$^{fl/fl}$-LysM-Cre* mice were effectively targeted *in vivo* resulting in similar increases in the amounts of LC3-I and p62, which indicate a defect in autophagy. Peritoneal MΦ and bronchoalveolar MΦ from *Atg14L$^{fl/fl}$-LysM-Cre* mice also accumulated p62 while, consistent with previous findings, the levels of LC3 were largely unaffected[12].

At 3 wpi, *Atg5$^{fl/fl}$* mice have higher bacterial titers as compared to C57Bl/6 mice (Fig. 1d, k), which we attribute to hypomorphic expression of *Atg5* from the *Atg5$^{fl/fl}$* allele (Extended Data Fig. 3 and [25]). To determine if germline hypomorphism for an essential ATG factor other than ATG5 interferes with control of *Mtb*, we infected mice that are hypomorphic for ATG16L1 (*Atg16L1^{HM1}*)[26] (Fig. 1m). *Atg16L1^{HM1}* mice showed no signs of sickness or weight loss following *Mtb* infection and controlled *Mtb* burden in a manner similar to C57Bl/6 mice (Fig. 1n–p, Extended Data Fig. 1c). Together, these data demonstrate that the loss of genes essential for canonical autophagy in LysM^{+} cells does not correlate with susceptibility to *Mtb* and suggest that ATG5 participates in a unique function not served by other essential ATG proteins. While autophagy-independent functions of ATG5 have been described[12–18], this is the first example of ATG5 being important for a response to an infection independent of ATG16L1 and ATG12.

To further explore how ATG5 functions during *Mtb* infection, we next investigated the reports that *Atg5$^{fl/fl}$-LysM-Cre* mice develop more severe inflammation following *Mtb* infection[4,9]. Various studies have demonstrated that myeloid-specific defects in components of the membrane elongation complex (ATG5, ATG7 or ATG16L1) can cause increased inflammation *in vivo*[27–29]. To distinguish between ATG16L1-dependent versus independent roles for ATG5 in regulating inflammation we measured immune responses to *Mtb* in the lungs of *Atg5$^{fl/fl}$-LysM-Cre*, *Atg16L1$^{fl/fl}$-LysM-Cre* and control mice. Phenotypes specific to loss of *Atg5* might be responsible for susceptibility to *Mtb* since *Atg16L1$^{fl/fl}$-LysM-Cre* mice control *Mtb* infection similarly to wild-type C57Bl/6 mice (Fig. 1). At 2 wpi, *Atg5$^{fl/fl}$-LysM-Cre* lungs contained larger lesions than those in C57Bl/6, *Atg5$^{fl/fl}$*, *Atg16L1$^{fl/fl}$-LysM-Cre* and *Atg16L1$^{fl/fl}$* mice (Fig. 2a), even though bacterial burdens were similar in each strain at this timepoint (Extended Data Fig. 4). By 3 wpi, *Atg5$^{fl/fl}$-LysM-Cre* lungs were severely inflamed with large lesions and extensive consolidation, while *Atg5$^{fl/fl}$* and *Atg16L1$^{fl/fl}$-LysM-Cre* lungs showed only moderate increases in inflammation (Fig. 2a). Consistent with this, the lungs of *Atg5$^{fl/fl}$-LysM-Cre* mice at 3 wpi contained higher levels of proinflammatory cytokines than *Atg16L1$^{fl/fl}$-LysM-Cre* or control mice (Fig. 2b). At this timepoint, the only cytokine that was significantly higher in the lungs of *Atg16L1$^{fl/fl}$-LysM-Cre* mice compared to controls was IL-1β, however this was still only half as much IL-1β as detected in *Atg5$^{fl/fl}$-LysM-Cre* lungs. The increased levels of IL-1β in mice lacking *Atg16L1* is consistent with previous reports showing that autophagy in MΦ negatively regulates inflammasome-dependent IL-1β production[9,27–29]. The observed differences in cytokine production were a specific and active response to *Mtb* infection, as cytokine levels were not

significantly different or were below the limit of detection in uninfected lungs (Extended Data Fig. 5).

To characterize cell populations contributing to the inflammation, flow cytometry was performed at 2 and 3 wpi in *Atg5*$^{fl/fl}$*-LysM-Cre*, *Atg16L1*$^{fl/fl}$*-LysM-Cre*, and control mice. At 2 wpi, *Atg5*$^{fl/fl}$*-LysM-Cre* lungs contained a significantly greater frequency of PMN than *Atg5*$^{fl/fl}$ or C57Bl/6 mice (Fig. 2c, Extended Data Fig. 6). This difference was more pronounced at 3 wpi, and at this time point the frequency of PMN in *Atg5*$^{fl/fl}$*-LysM-Cre* lungs was also significantly higher than in *Atg16L1*$^{fl/fl}$*-LysM-Cre* lungs (Fig. 2d). *Atg5*$^{fl/fl}$*-LysM-Cre* lungs also contained a greater percentage of inflammatory monocytes than C57Bl/6 mice at 2 wpi, however this level was similar to *Atg5*$^{fl/fl}$ lungs and, by 3 wpi, was not significantly different from any other strain. The increased inflammation in *Atg5*$^{fl/fl}$*-LysM-Cre* lungs likely contributes to the severe lung pathology and morbidity observed in these mice (Fig. 1a, b and Fig. 2a–d). In addition, the absence of higher bacterial burden at 2 wpi (Extended Data Fig. 4) indicates that the increased inflammation in the *Mtb* infected *Atg5*$^{fl/fl}$*-LysM-Cre* mice is a direct result of loss of *Atg5* rather than a response to uncontrolled bacterial replication.

Excessive PMN recruitment is a hallmark of acute susceptibility to *Mtb* and is associated with uncontrolled tissue damage and progression of disease[11]. We hypothesized that the susceptibility of the *Atg5*$^{fl/fl}$*-LysM-Cre* mice is related to the increased frequency of PMN in these mice during *Mtb* infection and, therefore, sought to determine if depletion of PMN would improve control of *Mtb*[11]. Antibody-mediated depletion of PMN (anti-Ly6G, clone 1A8) from 10 – 28 dpi allowed *Atg5*$^{fl/fl}$*-LysM-Cre* mice to recover their loss in weight and survive over 80 dpi (Fig. 3a, b). To survive 80 dpi, PMN-depleted *Atg5*$^{fl/fl}$*-LysM-Cre* mice must have functional IFN-γ signaling and T cell responses, since *Rag*$^{-/-}$ and PMN-depleted *IFNGR*$^{-/-}$ mice both succumb to *Mtb* by 60 dpi[11]. Furthermore, at 3 wpi, PMN-depleted *Atg5*$^{fl/fl}$*-LysM-Cre* mice had significantly lower levels of proinflammatory cytokines, pulmonary burden, and lung pathology than IgG control-treated mice (Fig. 3c–e). The depletion of PMN alleviated all phenotypes observed at 3 wpi in *Atg5*$^{fl/fl}$*-LysM-Cre* mice, indicating that a dysfunctional PMN response leads to the susceptibility of these mice.

We next sought to determine in which cell type(s) *Atg5* is required to control *Mtb*. *LysM-Cre* deletion occurs in PMN, MΦ, inflammatory monocytes and myeloid-derived DC[19,20], indicating that *Atg5* plays a critical role in one or more of these populations during *Mtb* infection. Alveolar MΦ are the first cells infected upon inhalation of *Mtb* and are required for the establishment of infection[30]. Furthermore, previous *in vitro* studies suggested that a predominant role for ATG5 during *Mtb* infection is to control bacterial replication in MΦ[1–4,6–8]. Therefore, we investigated whether ATG5 is required in alveolar MΦ to control *Mtb* by infecting *Atg5*$^{fl/fl}$*-CD11c-Cre* mice, which lack ATG5 in alveolar MΦ and DC[20]. In contrast to *Atg5*$^{fl/fl}$*-LysM-Cre* mice, *Atg5*$^{fl/fl}$*-CD11c-Cre* mice did not lose weight during *Mtb* infection, were able to control bacterial burden, and survived over 80 dpi (Fig. 4a–c). Alveolar MΦ from *Atg5*$^{fl/fl}$*-CD11c-Cre* and *Atg5*$^{fl/fl}$*-LysM-Cre* mice displayed similar autophagy defects (Fig. 4d and Extended Data Fig. 2), indicating that resistance to *Mtb* is neither dependent on nor correlated with autophagic capacity in alveolar MΦ. Furthermore, this suggests ATG5 plays an essential role within other cells targeted by *LysM-Cre*-mediated

gene deletion, such as PMNs, recruited MΦ and/or inflammatory monocytes, to control *Mtb* infection.

We have shown that excessive PMN dominated inflammation leads to the susceptibility of *Atg5*$^{fl/fl}$*-LysM-Cre* mice. To determine whether loss of *Atg5* from PMN is sufficient to cause susceptibility to *Mtb*, we next utilized *Atg5*$^{fl/fl}$*-MRP8-Cre* mice, which delete *Atg5* in PMN[20] (Fig. 4e). *Atg5*$^{fl/fl}$*-MRP8-Cre* mice were more susceptible to *Mtb* infection, as indicated by an average increase in weight loss compared to floxed controls (Fig. 4f). However, analysis of individual mice revealed that only half of the *Atg5*$^{fl/fl}$*-MRP8-Cre* mice lost weight following *Mtb* infection (between 10 – 20% of their starting weight); the remaining 50% of mice exhibited an average 2% weight gain. This split phenotype was reproducible across multiple experiments, and was independent of differences in age, sex, or litter of the mice, suggesting a threshold effect in the susceptibility of the *Atg5*$^{fl/fl}$*-MRP8-Cre* mice. To study these two distinct outcomes, we compared responses in mice that lost over 5% of their starting weight at 20 dpi ("susceptible") with the remaining mice ("healthy") (Fig. 4g). At 3 wpi, lungs from susceptible *Atg5*$^{fl/fl}$*-MRP8-Cre* mice exhibited higher bacterial burden, cytokine responses, and frequency of PMN (Fig. 4h–j, Extended Data Fig. 7). The susceptible *Atg5*$^{fl/fl}$*-MRP8-Cre* mice display the same phenotypes as the *Atg5*$^{fl/fl}$*-LysM-Cre* mice, demonstrating a PMN-intrinsic role for ATG5 during acute *Mtb* infection. However, the incomplete penetrance of susceptibility in *Atg5*$^{fl/fl}$*-MRP8-Cre* mice suggests that the extreme sensitivity of *Atg5*$^{fl/fl}$*-LysM-Cre* mice to *Mtb* results from the loss of *Atg5* in MΦ and monocytes, as well as PMN. Notably, *Atg16L1*$^{fl/fl}$*-LysM-Cre* mice are not susceptible to *Mtb* infection even though PMN (Extended Data Fig. 8), in addition to MΦ (Fig. 1l and Extended Data Fig. 2), from *Atg16L1*$^{fl/fl}$*-LysM-Cre* and *Atg5*$^{fl/fl}$*-LysM-Cre* mice have a similar defect in autophagy. This further supports that ATG5 functions, at least in part, independently of ATG16L1 to protect mice from *Mtb* infection.

Despite numerous *in vitro* studies emphasizing a role for autophagy in MΦ during *Mtb* infection (including, but not limited to ref [1–8]), our data show that loss of genes essential for canonical autophagy does not correlate with susceptibility to *Mtb* in the context of a complete immune response in the host. Importantly, mice used in our studies have similar autophagy defects and have been used in prior publications to investigate the function of individual ATG factors[12–15], validating these mice as suitable genetic models to study autophagy *in vivo*. Our studies indicate that prior reports analyzing the role of only a single autophagy gene to conclude that canonical autophagy is responsible for the phenotypes observed need to be reexamined. The observation that the *Atg5*$^{fl/fl}$ and *Atg5*$^{fl/fl}$*-LysM-Cre* mice have only small differences in *Mtb* burden supports the other data presented herein that the dramatic difference in the inflammatory response is the predominant driver of susceptibility in *Atg5*$^{fl/fl}$*-LysM-Cre* mice during *Mtb* infection. The apparent insignificance of macroautophagy for controlling *Mtb* replication may reflect that *Mtb* encodes highly effective inhibitors of canonical autophagy, however these mechanisms have yet to be described. Furthermore, studies investigating loss of autophagy, including this one, do not address whether activation of autophagy could enhance restriction of *Mtb* replication.

By analyzing different Cre-mediated deletion strains, we have found that loss of *Atg5* in PMN, but not alveolar MΦ or DC, can result in loss of control of *Mtb* infection, but the

severe susceptibility of the *Atg5$^{fl/fl}$-LysM-Cre* mice relies on deletion of *Atg5* in multiple LysM^{+} cell types. These data also reveal a PMN-intrinsic role for ATG5 during *Mtb* infection. Importantly, the reversal of all phenotypes in the *Atg5$^{fl/fl}$-LysM-Cre* mice upon PMN-depletion positions PMN as a major driver in the dysfunctional response in these mice. Our experiments point to a model where infection with *Mtb* induces a proinflammatory response that leads to the recruitment of PMN to the lung. The absence of *Atg5* expression within the responding myeloid cells leads to uncontrolled accumulation of PMN in the lung, which causes increased pathology and likely provides an expanded niche for bacterial infection. The animal then succumbs to infection before the adaptive immune response is able to control the inflammation and bacterial replication. Together, the *in vivo* genetic analyses presented here argue for a shift in focus onto macroautophagy-independent roles of ATG5 in controlling resistance to *Mtb* infection *in vivo*.

Methods

Cells and Media

Mycobacterium tuberculosis Erdman was cultured at 37 C in 7H9 (broth) or 7H10 (agar) (Difco) medium supplemented with 10% oleic acid/albumin/dextrose/catalase (OADC), 0.5% glycerol, and 0.05% Tween 80 (broth).

Ex vivo MΦ were enriched from mice via bronchoalveolar lavage or peritoneal lavage with DMEM + 10% FBS + 1% MEM non-essential amino acids (Cellgro 25–025-CI) + 100 U/mL Penicillin + 100 mg/mL Streptomycin (Sigma P4333). Lavage cells were treated with ACK lysis buffer (0.15M NH_4Cl, 10mM $KHCO_3$, 0.1mM EDTA) to lyse red blood cells, plated in tissue culture treated plates, and incubated at 37°C in 5% CO_2 for at least 4 hours to allow adherence of MΦ[14]. Wells were washed vigorously with PBS to remove non-adherent cells and lysed in 2X Laemmli buffer for western blot analysis.

Bone marrow derived MΦ were isolated from femurs and tibias of mice, and cultured in DMEM + 20% FBS + 10% supernatant from 3T3 cells overexpressing M-CSF + 1% MEM non-essential amino acids (Cellgro 25–025-CI) + 100 U/mL penicillin and 100 μg/mL streptomycin (Sigma P4333) at 37° C in 5% CO_2.

PMN for *ex vivo* western blotting analysis were purified from uninfected bone marrow by negative selection via MACS column (Miltenyi Biotech, 130-097-658) according to manufacturer's guidelines and immediately lysed in 2X Laemmi buffer.

Western Blotting

Protein samples were diluted in 2X Laemmli buffer, resolved using 4–20% polyacrylamide gels (BioRad #456-1096) transferred to PVDF membrane (GE Healthcare 10600023) and detected with the following antibodies: LC3b (Sigma L7543 - detects LC3-I and LC3-II), p62 / *SQSTM1* (Sigma P0067), ATG5 (Sigma A2859), β-actin (Cell Signaling Technology #4970) and goat-anti-mouse:HRP and goat-anti-rabbit:HRP as appropriate. HRP was detected using Western Lightning Plus ECL (PerkinElmer #NEL103001EA) for actin or ECL Prime (GE Healthcare RPN2232) for LC3b, p62 and ATG5. For gel source data, see Supplementary Figure 1.

Mouse strains

Adult mice (age 7–15 weeks) of both sexes were used and mouse experiments were randomized. No blinding was performed during animal experiments. All mice used have been fully backcrossed to a C57Bl/6 background. Sample sizes are detailed in Supplemental Figure 2 and were sufficient to detect differences as small as 10% using the statistical methods described. *Atg5$^{fl/fl}$-LysM-Cre, Atg7$^{fl/fl}$-LysM-Cre, Atg16L1$^{fl/fl}$-LysM-Cre, Atg3$^{fl/fl}$-LysM-Cre*, and *Atg14L1$^{fl/fl}$-LysM-Cre*, and all floxed control mice have been previously described[12–14]. *Atg14L$^{fl/fl}$-LysM-Cre* and floxed control mice were kindly provided by Dr. Shizuo Akira, Osaka University, Japan. *Atg3$^{fl/fl}$-LysM-Cre* mice were derived from *Atg3$^{fl/fl}$* mice kindly provided by Dr. You-Wen He, Duke University, USA[31]. *Atg12$^{fl/fl}$-LysM-Cre* mice were derived from *Atg12$^{fl/fl}$* mice[32]. *Atg16L1^{HM1}* mice have been previously described (HM1, BC0122 strain)[26]. *p62$^{-/-}$* mice were kindly supplied by Dr. Eileen White at Rutgers University[33]. *Atg4B$^{gt/gt}$* mice were previously described, and are referred to as *Atg4B$^{-/-}$* throughout the text[24]. *Ulk1$^{-/-}$* and *Ulk2$^{-/-}$* mice were kindly provided by Dr. Sharon Tooze at the London Research Institute[34,35]. *Atg5$^{fl/fl}$-CD11c-Cre* and *Atg5$^{fl/fl}$-MRP8-Cre* mice were generated in our facility by crossing *Atg5$^{fl/fl}$* to *CD11c-Cre* (The Jackson Laboratory 007567) and *MRP8-Cre* (The Jackson Laboratory 021614).

All procedures involving animals were conducted following the National Institute of Health guidelines for housing and care of laboratory animals and performed in accordance with institutional regulations after protocol review and approval by the Institutional Animal Care and Use Committee of The Washington University in St. Louis School of Medicine (protocol #20130156, Analysis of Mycobacterial Pathogenesis). Washington University is registered as a research facility with the United States Department of Agriculture and is fully accredited by the American Association of Accreditation of Laboratory Animal Care. The Animal Welfare Assurance is on file with OPRR-NIH. All animals used in these experiments were subjected to no or minimal discomfort. All mice were euthanized by CO_2 asphyxiation, which is approved by The Panel on Euthanasia of the American Veterinary Association.

Mtb infection of mice

Before infection, exponentially replicating *Mtb* were washed in PBS + 0.05% Tween-80, and sonicated to disperse clumps. 7- to 15-week-old female and male mice were exposed to 8×10^7 colony forming units (CFU) of *Mtb* in an Inhalation Exposure System (Glas-Col), which delivers ~100 bacteria to the lung per animal. At 24 hours post infection, the bacterial titers in the lungs of at least two mice were determined to confirm the dose of *Mtb* inoculation. The dose determined from these mice is assumed to represent the average dose received by all mice in the same infection. Bacterial burden was determined by plating serial dilutions of lung homogenates onto 7H10 agar plates. Plates were incubated at 37°C in 5% CO_2 for 3 weeks prior to counting colonies.

Flow cytometry

Lungs were perfused with sterile PBS and digested at 37°C for 1 hour with 625 μg/mL collagenase D (Roche 11088875103) and 75 U/mL DNase I (Sigma D4527). Single cell suspensions stained in PBS + 2% FBS + 0.1% sodium azide in the presence of Fc receptor

blocking antibody (BD Pharmingen 553541) and stained with the antibodies against the following mouse markers: CD11b_PerCP-Cy5.5 (BD Pharmingen 550993), CD11c_APC-Cy7 (eBioscience 47-0114), Ly6C_PE (BD Pharmingen 560592), Ly6G_PE-Cy7 (BD Pharmingen 560601), and F4/80_APC (Invitrogen MF48005). The FITC channel was used to determine autofluorescence. Cells were stained for 20 minutes at 4C and then fixed in 4% paraformaldehyde (Electron Microscopy Sciences) for 20 minutes at room temperature. Flow cytometry was performed on a FACSCanto II (BD Bioscience) and data was analyzed with FlowJo (Tree Star Inc.). Gating strategies are depicted in Extended Data Fig. 6a.

Cytokine analysis

Lungs (right lobe) were homogenized in 1mL (uninfected mice) or 5mL (*Mtb*-infected mice) PBS + 0.05% Tween-80. Homogenized tissue supernatants were filtered (0.22um) and analyzed by ELISA according to manufacturer's guidelines (R&D systems): KC/CXCL1 (DY453), IFN-γ (DY485), TNF-α (DY410), IL-1α (DY400), IL-1α (DY401), IL-6 (DY406), IL-17 (DY421), MIP-1α/CCL3 (DY450), MIP-2/CXCL2 (DY452), and G-CSF (DY414).

RNA extraction and quantification

Following tissue disruption by bead-beating (MP Biosystems), RNA was extracted from *Mtb*-infected lungs using the RNeasy Kit according to manufacturer's guidelines (Qiagen 74106). cDNA was made with SuperScript III reverse transcriptase using oligo-dT primers (Life Technologies 18080-051). qRT-PCR was performed using iTAQ SYBR Green (BioRad 172-5121) and transcript levels were normalized to actin. The following primers were used: *Atg16L1-fwd* 5′-CCGAATCTGGACTGTGGATG-3′, *Atg16L1-rev* 5′CGGAGATCCCAGAGTTTGAG-3′, *Actin-fwd* 5′-ACCTTCTACAATGAGCTGCG-3′, and *Actin-rev* 5′-CTGGATGGCTACGTACATGG-3′

PMN depletion

Mice were treated with 0.2 mg anti-Ly6G (clone 1A8) or 0.2 mg rat IgG (Sigma I8015) via i.p. injection every 48 hours between day 10 and 28 post infection. Efficacy of PMN depletion was confirmed by loss of $CD11b^{+}$ $Gr\text{-}1^{high}$ cells in lungs at 21 dpi. Anti-Ly6G was collected from 1A8 hybridoma[36] grown in Serum Free Medium (Gibco #12045-076) in CL350 Bioreactor flasks (Argos Technologies #900 10).

Data and Statistics

All experiments were performed at least twice. When shown, multiple samples represent biological (not technical) replicates of mice randomly sorted into each experimental group. No blinding was performed during animal experiments. Animals were only excluded when pathology unrelated to *Mtb* infection was present (i.e. weight loss due to malocculsion). Determination of statistical differences was performed with Prism 5 (Graphpad Software, Inc) using log-rank Mantel-Cox test (survival), unpaired two-tailed t-test (to compare two groups with similar variances), or one-way ANOVA with Bonferonni's Multiple Comparison test (to compare more than two groups). Sample sizes were sufficient to detect differences as small as 10% using the statistical methods described. When used, center values and error bars represent the mean ± S.E.M. In all figures, all significant differences are indicated by

asterisks: * $P < 0.05$, ** $P < 0.01$, *** $P < 0.001$, **** $P < 0.0001$. Non-significant comparisons of particular interest are noted in figures by n.s. (not significant). Sample sizes and the results of all comparisons can be found in Supplementary Figure 2.

Extended Data

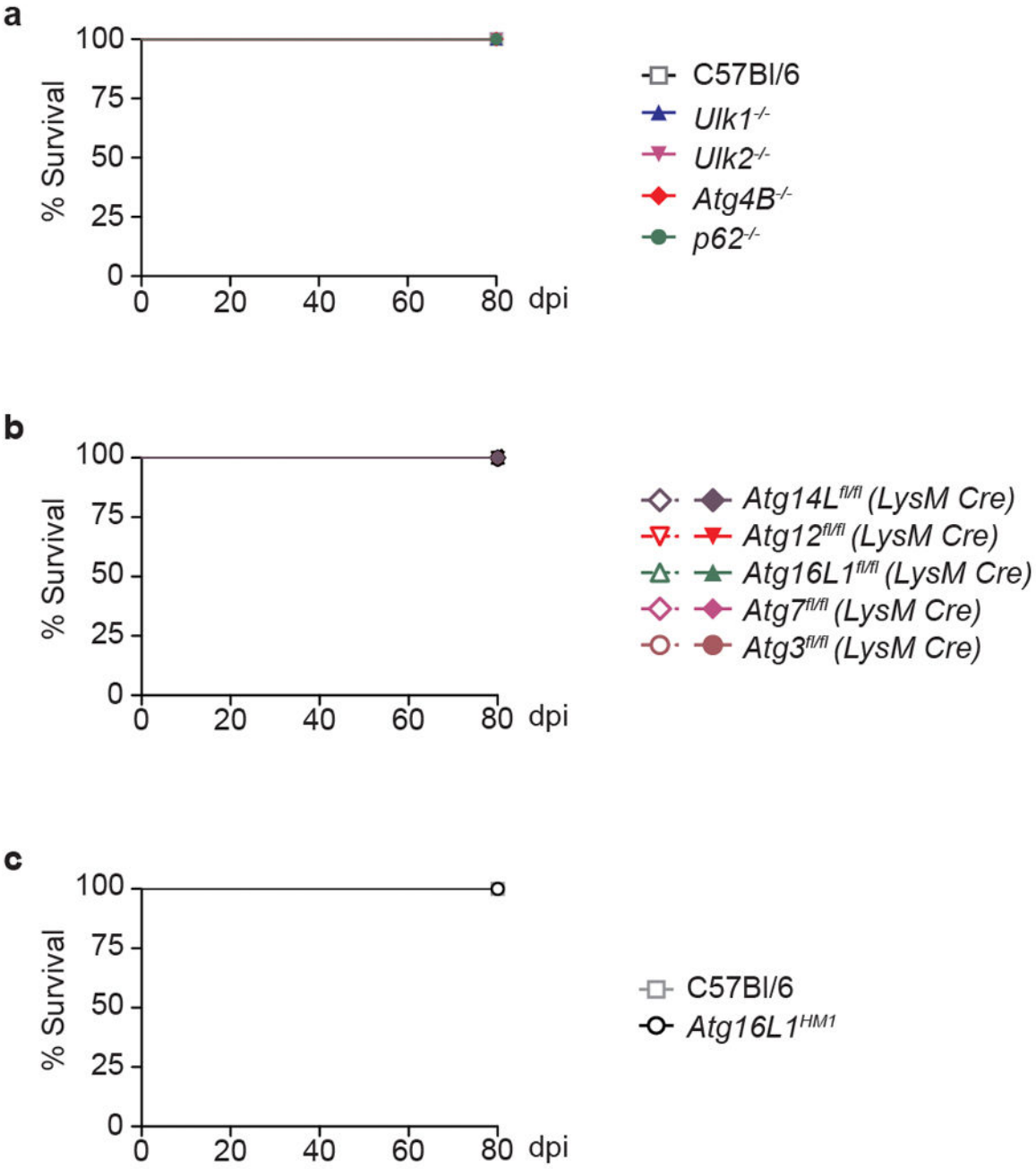

Extended Data Figure 1. Survival of mice with defects in autophagy genes other than *Atg5*

Percent survival of mice following infection with 100 CFU of aerosolized *Mtb.* **a**, Survival of C57Bl/6 (open squares), *Ulk1*$^{-/-}$ (blue triangles), *Ulk2*$^{-/-}$ (inverted pink triangles),

Atg4B$^{-/-}$ (red diamonds), and *p62*$^{-/-}$ (green circles) mice. **b**, Survival of *Atg14L*$^{fl/fl}$*-LysM-Cre* (purple diamonds), *Atg12*$^{fl/fl}$*-LysM-Cre* (red inverted triangles), *Atg16L1*$^{fl/fl}$*-LysM-Cre* (green triangles), *Atg7*$^{fl/fl}$*-LysM-Cre* (pink diamonds), *Atg3*$^{fl/fl}$*-LysM-Cre* (brown circles) and corresponding floxed control mice. Floxed control mice are shown in open shapes, LysM-Cre-expressing mice are shown in closed shapes. **c**, Survival of C57Bl/6 (open squares), *Atg16L1*^{HM1} (open circles). Samples represent biological replicates. See Supplementary Figure 2 for sample sizes.

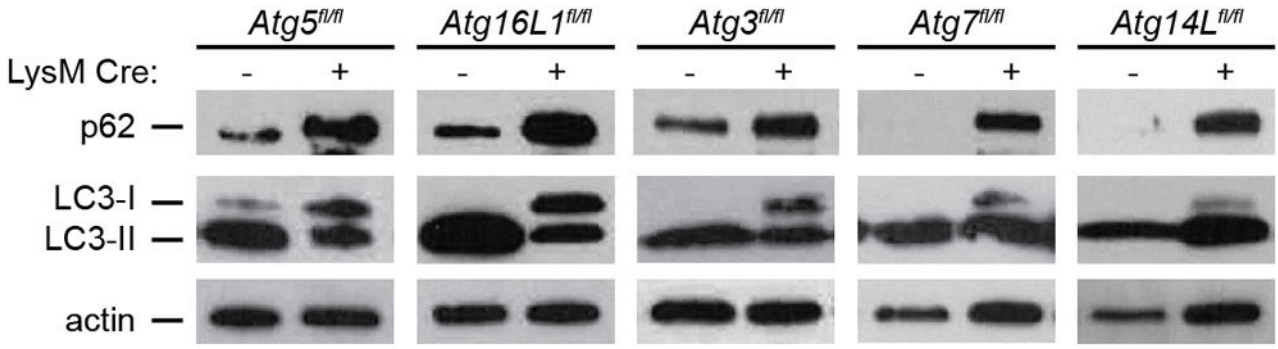

Extended Data Figure 2. Analysis of autophagy in bronchoalveolar MΦ

Western blot analysis of p62, LC3, and actin levels in *ex vivo* macrophages isolated from bronchoalveolar lavages of uninfected mice. For gel source data, see Supplementary Figure 1.

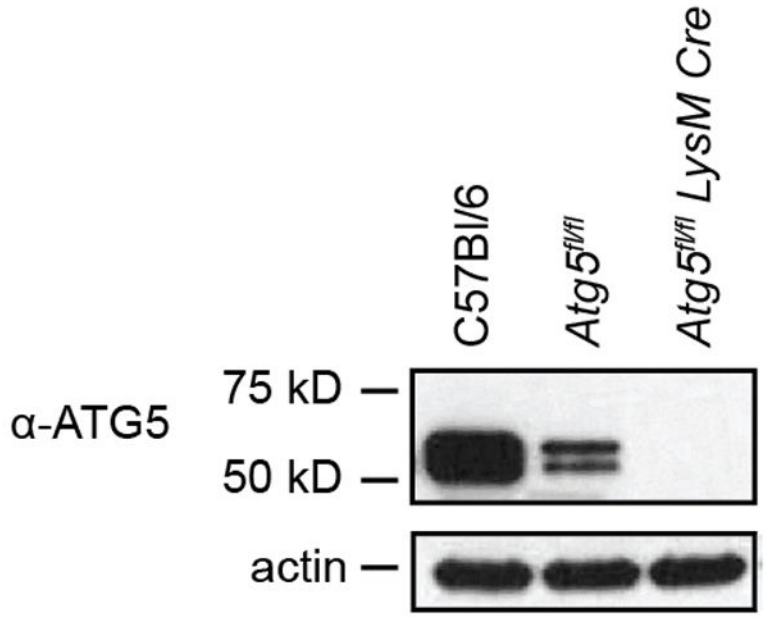

Extended Data Figure 3. *Atg5*$^{fl/fl}$ bone marrow derived MΦ are hypomorphic for ATG5

Western blot analysis of ATG5 (ATG5–ATG12 conjugate, 56 kDa) and actin in uninfected bone marrow derived MΦ. For gel source data, see Supplementary Figure 1.

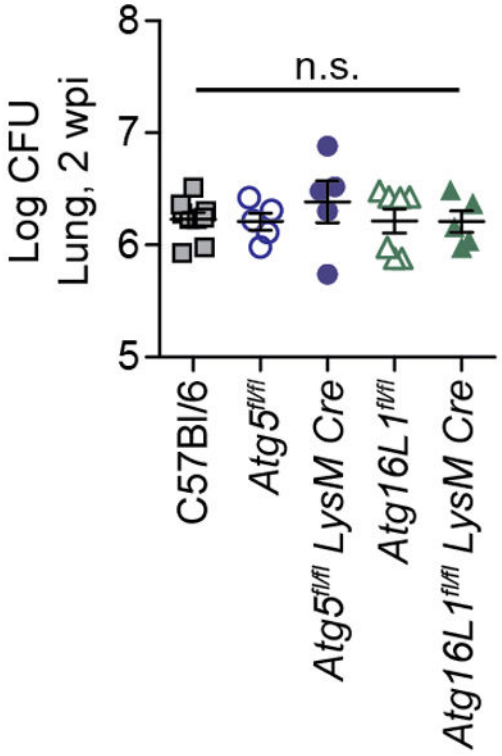

Extended Data Figure 4. Loss of *Atg5* or *Atg16L1* in LysM$^+$ cells does not lead to increased CFU at 2 wpi

Log pulmonary CFU at 2 weeks post infection (wpi). Samples represent biological replicates.

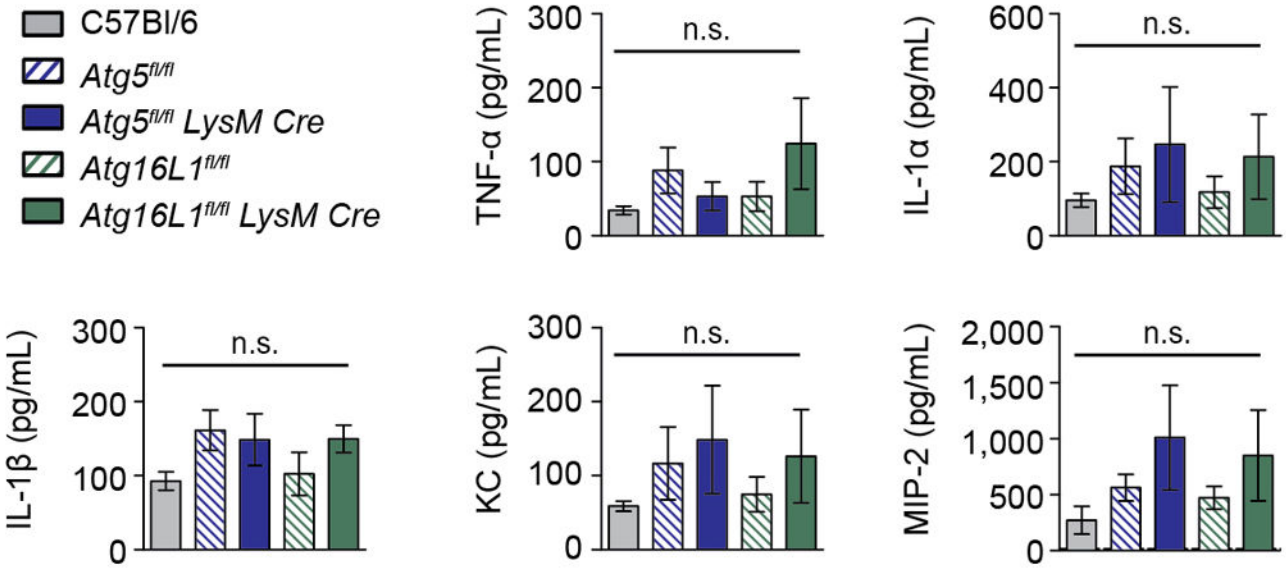

Extended Data Figure 5. Cytokine levels in uninfected lungs

Concentration of cytokines in lungs (homogenized in 1mL) from uninfected mice. Levels of IFN-γ, IL-6, MIP-1α, IL-17, and G-CSF were below the limit of detection. C57Bl/6 (grey

solid bars), *Atg5*$^{fl/fl}$ (blue striped bars), *Atg5*$^{fl/fl}$*-LysM-Cre* (blue solid bars), *Atg16L1*$^{fl/fl}$ (green striped bars), *Atg16L1*$^{fl/fl}$*-LysM-Cre* (green solid bars). Statistical differences were determined by one-way ANOVA and Bonferonni's multiple comparison test. n.s., not significant. Samples represent biological replicates. See Supplementary Figure 2 for sample sizes and results from all statistical comparisons.

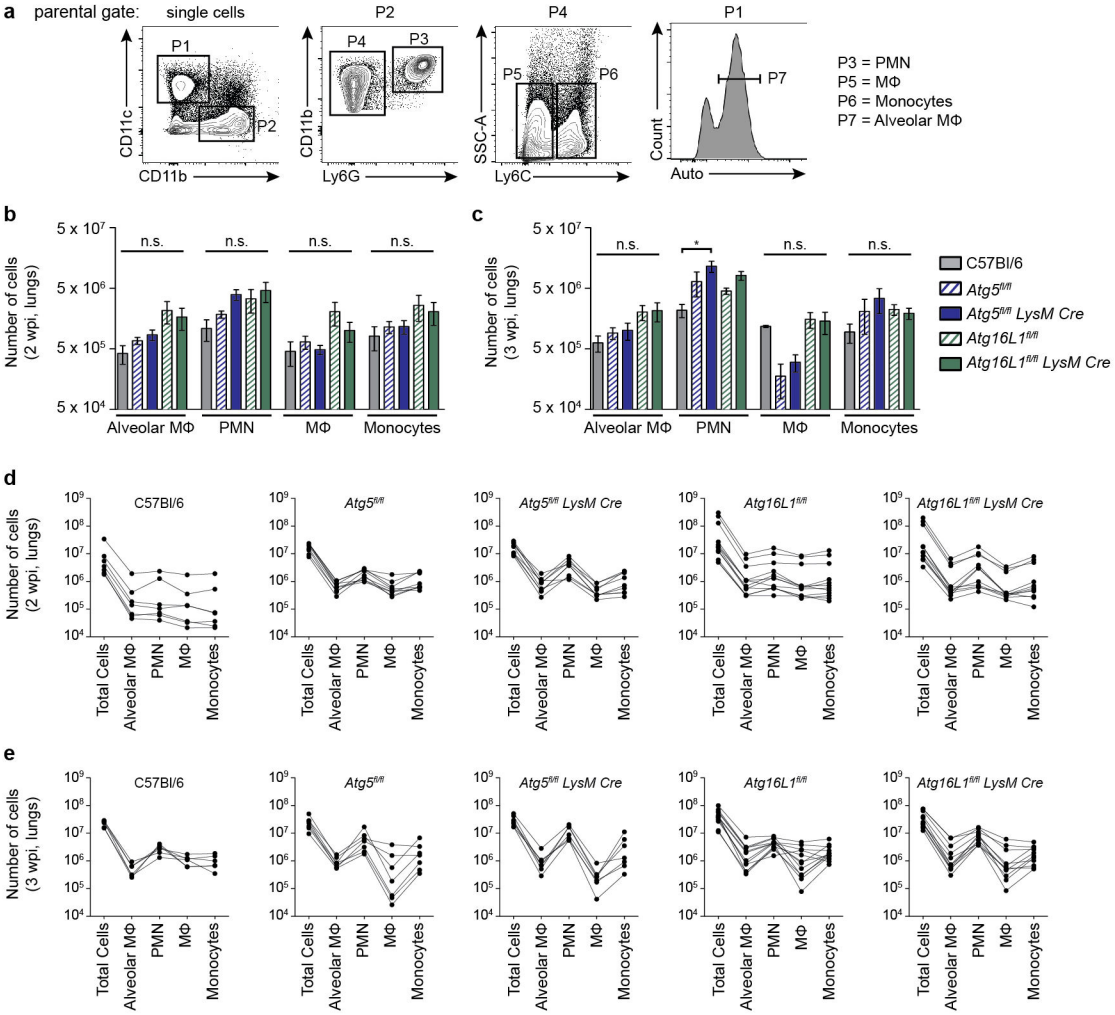

Extended Data Figure 6. Number of inflammatory cells in lungs of mice at 2 and 3 wpi (related to Fig. 2)

a, Gating strategy for analysis of inflammatory cells in lungs at 2 and 3 wpi. Single lung cells were gated based on CD11b, CD11c, Ly6G, Ly6C and autofluorescence (auto). The parental gate is shown above each contour plot. Representative data is shown from an *Atg5*$^{fl/fl}$ mouse at 2 wpi. **b, c,** C57Bl/6 (grey solid bars), *Atg5*$^{fl/fl}$ (blue striped bars), *Atg5*$^{fl/fl}$*-LysM-Cre* (blue solid bars), *Atg16L1*$^{fl/fl}$ (green striped bars), *Atg16L1*$^{fl/fl}$*-LysM-Cre* (green solid bars). Mean number of alveolar MΦ, PMN, recruited MΦ, and inflammatory monocytes in lungs at 2 wpi (**b**) and 3 wpi (**c**). Flow cytometry data presented in (**b**) and (**c**) and in Fig. 2 are the compilation of results from five experiments. In some experiments, different amounts of lung were collected for analysis, making it difficult to

compare the average number of each cells between strains, unless the data is normalized (as done in Fig. 2c, d – percentage of total cells). Therefore, to compare the raw number of cells detected in each cell population, each mouse analyzed at 2 wpi (**d**) and 3 wpi (**e**) has been graphed individually. Each line represents a different mouse, with dots indicating the number of total cells, alveolar MΦ, PMN, recruited MΦ and inflammatory monocytes. Statistical differences were determined by one-way ANOVA and Bonferonni's multiple comparison test (**b, c**). * $P < 0.05$. Notable comparisons that were not significantly different are designated as n.s. Samples represent biological replicates. See Supplementary Figure 2 for sample sizes and results from all statistical comparisons.

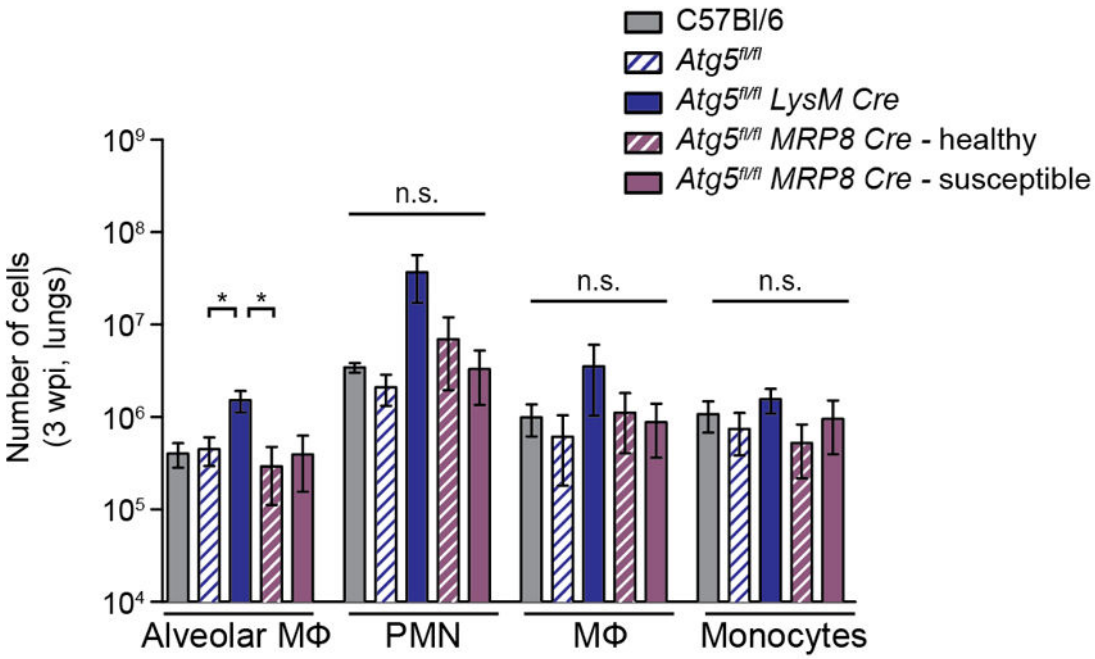

Extended Data Figure 7. Number of inflammatory cells in lungs of mice at 3 wpi (related to Fig. 4)

Number of alveolar MΦ, PMN, recruited MΦ, and inflammatory monocytes in lungs at 3 wpi. C57Bl/6 (grey solid bars), *Atg5*$^{fl/fl}$ (blue striped bars), *Atg5*$^{fl/fl}$*-LysM-Cre* (blue solid bars), "healthy" *Atg5*$^{fl/fl}$*-MRP8-Cre* (purple striped bars), and "susceptible" *Atg5*$^{fl/fl}$*-MRP8-Cre* (purple solid bars). Statistical differences were determined by one-way ANOVA and Bonferonni's multiple comparison test * $P < 0.05$. Notable comparisons that were not significantly different are designated as n.s. Samples represent biological replicates. See Supplementary Figure 2 for sample sizes and results from all statistical comparisons.

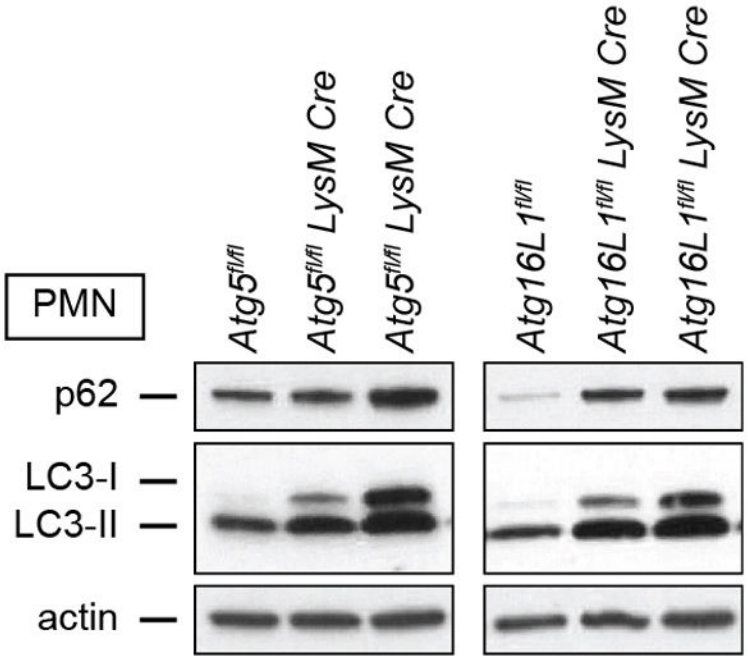

Extended Data Figure 8. Analysis of autophagy in bone marrow PMN

Western blot analysis of p62, LC3, and actin in bone marrow PMN from uninfected mice. Each lane represents an individual mouse. Two replicates of the *Atg5$^{fl/fl}$-LysM-Cre* and *Atg16L1$^{fl/fl}$-LysM-Cre* mice are shown. For gel source data, see Supplementary Figure 1.

Supplementary Material

Refer to Web version on PubMed Central for supplementary material.

Acknowledgments

C.L.S. is supported by a Beckman Young Investigator Award from the Arnold and Mabel Beckman Foundation. J.M.K. is supported by a National Science Foundation Graduate Research Fellowship DGE-1143954 and the NIGMS Cell and Molecular Biology Training Grant GM007067. J.P.H. is supported by a National Science Foundation Graduate Research Fellowship DGE-1143954. H.W.V., S.P., and A.K. are supported by U19 AI109725. We would like to acknowledge Darren Kreamalmeyer for assistance with the mouse colonies and Dr. Thomas Malek and Dr. L. David Sibley for providing the 1A8 hybridoma.

References

1. Deretic V. Autophagy in Tuberculosis. Cold Spring Harbor Perspectives in Medicine. 2014; doi: 10.1101/cshperspect.a018481
2. Dutta RK, Kathania M, Raje M, Majumdar S. IL-6 inhibits IFN-γ induced autophagy in Mycobacterium tuberculosis H37Rv infected macrophages. Int J Biochem Cell Biol. 2012; 44:942–954. [PubMed: 22426116]
3. Juárez E, et al. NOD2 enhances the innate response of alveolar macrophages to Mycobacterium tuberculosis in humans. Eur J Immunol. 2012; 42:880–889. [PubMed: 22531915]
4. Watson RO, Manzanillo PS, Cox JS. Extracellular M. tuberculosis DNA Targets Bacteria for Autophagy by Activating the Host DNA-Sensing Pathway. Cell. 2012; 150:803–815. [PubMed: 22901810]

5. Seto S, Tsujimura K, Horii T, Koide Y. Autophagy Adaptor Protein p62/SQSTM1 and Autophagy-Related Gene Atg5 Mediate Autophagosome Formation in Response to Mycobacterium tuberculosis Infection in Dendritic Cells. PLoS ONE. 2013; 8:e86017. [PubMed: 24376899]
6. Sakowski ET, et al. Ubiquilin 1 Promotes IFN-γ-Induced Xenophagy of Mycobacterium tuberculosis. PLoS Pathog. 2015; 11:e1005076. [PubMed: 26225865]
7. Gutierrez MG, et al. Autophagy is a defense mechanism inhibiting BCG and Mycobacterium tuberculosis survival in infected macrophages. Cell. 2004; 119:753–766. [PubMed: 15607973]
8. Wang J, et al. MicroRNA-155 Promotes Autophagy to Eliminate Intracellular Mycobacteria by Targeting Rheb. PLoS Pathog. 2013; 9:e1003697. [PubMed: 24130493]
9. Castillo EF, et al. Autophagy protects against active tuberculosis by suppressing bacterial burden and inflammation. Proc Natl Acad Sci USA. 2012; 109:E3168–E3176. [PubMed: 23093667]
10. Cooper AM, et al. Disseminated tuberculosis in interferon gamma gene-disrupted mice. J Exp Med. 1993; 178:2243–2247. [PubMed: 8245795]
11. Nandi B, Behar SM. Regulation of neutrophils by interferon-γ limits lung inflammation during tuberculosis infection. Journal of Experimental Medicine. 2011; 208:2251–2262. [PubMed: 21967766]
12. Choi J, et al. The Parasitophorous Vacuole Membrane of Toxoplasma gondii Is Targeted for Disruption by Ubiquitin-like Conjugation Systems of Autophagy. Immunity. 2014; 40:924–935. [PubMed: 24931121]
13. Hwang S, et al. Nondegradative Role of Atg5-Atg12/ Atg16L1 Autophagy Protein Complex in Antiviral Activity of Interferon Gamma. Cell Host and Microbe. 2012; 11:397–409. [PubMed: 22520467]
14. Zhao Z, et al. Autophagosome-Independent Essential Function for the Autophagy Protein Atg5 in Cellular Immunity to Intracellular Pathogens. Cell Host and Microbe. 2008; 4:458–469. [PubMed: 18996346]
15. Martinez J, et al. Molecular characterization of LC3-associated phagocytosis reveals distinct roles for Rubicon, NOX2 and autophagy proteins. Nat Cell Biol. 2015; 17:893–906. [PubMed: 26098576]
16. Jounai N, et al. The Atg5 Atg12 conjugate associates with innate antiviral immune responses. Proc Natl Acad Sci USA. 2007; 104:14050–14055. [PubMed: 17709747]
17. Yousefi S, et al. Calpain-mediated cleavage of Atg5 switches autophagy to apoptosis. Nat Cell Biol. 2006; 8:1124–1132. [PubMed: 16998475]
18. Maskey D, et al. ATG5 is induced by DNA-damaging agents and promotes mitotic catastrophe independent of autophagy. Nat Commun. 2013; 4:2130. [PubMed: 23945651]
19. Jakubzick C, et al. Lymph-migrating, tissue-derived dendritic cells are minor constituents within steady-state lymph nodes. Journal of Experimental Medicine. 2008; 205:2839–2850. [PubMed: 18981237]
20. Abram CL, Roberge GL, Hu Y, Lowell CA. Comparative analysis of the efficiency and specificity of myeloid-Cre deleting strains using ROSA-EYFP reporter mice. J Immunol Methods. 2014; 408:89–100. [PubMed: 24857755]
21. Flynn JL, Chan J. Immunology of tuberculosis. Annu Rev Immunol. 2001; 19:93–129. [PubMed: 11244032]
22. Jayaswal S, et al. Identification of Host-Dependent Survival Factors for Intracellular Mycobacterium tuberculosis through an siRNA Screen. PLoS Pathog. 2010; 6:e1000839. [PubMed: 20419122]
23. Jung CH, et al. ULK-Atg13-FIP200 complexes mediate mTOR signaling to the autophagy machinery. Mol Biol Cell. 2009; 20:1992–2003. [PubMed: 19225151]
24. Mariño G, et al. Autophagy is essential for mouse sense of balance. J Clin Invest. 2010; 120:2331–2344. [PubMed: 20577052]
25. Lin HH, et al. Dynamic involvement of ATG5 in cellular stress responses. Cell Death Dis. 2014; 5:e1478. [PubMed: 25341032]
26. Cadwell K, et al. A key role for autophagy and the autophagy gene Atg16l1 in mouse and human intestinal Paneth cells. Nature. 2008; 456:259–263. [PubMed: 18849966]

27. Abdel Fattah E, Bhattacharya A, Herron A, Safdar Z, Eissa NT. Critical role for IL-18 in spontaneous lung inflammation caused by autophagy deficiency. J Immunol. 2015; 194:5407–5416. [PubMed: 25888640]
28. Kanayama M, He YW, Shinohara ML. The lung is protected from spontaneous inflammation by autophagy in myeloid cells. J Immunol. 2015; 194:5465–5471. [PubMed: 25911758]
29. Saitoh T, et al. Loss of the autophagy protein Atg16L1 enhances endotoxin-induced IL-1beta production. Nature. 2008; 456:264–268. [PubMed: 18849965]
30. Leemans JC, et al. Depletion of alveolar macrophages exerts protective effects in pulmonary tuberculosis in mice. J Immunol. 2001; 166:4604–4611. [PubMed: 11254718]
31. Jia W, He YW. Temporal regulation of intracellular organelle homeostasis in T lymphocytes by autophagy. J Immunol. 2011; 186:5313–5322. [PubMed: 21421856]
32. Malhotra R, Warne JP, Salas E, Xu AW, Debnath J. Loss of Atg12, but not Atg5, in pro-opiomelanocortin neurons exacerbates diet-induced obesity. Autophagy. 2015; 11:145–154. [PubMed: 25585051]
33. Komatsu M, et al. Homeostatic levels of p62 control cytoplasmic inclusion body formation in autophagy-deficient mice. Cell. 2007; 131:1149–1163. [PubMed: 18083104]
34. Lee EJ, Tournier C. The requirement of uncoordinated 51-like kinase 1 (ULK1) and ULK2 in the regulation of autophagy. Autophagy. 2011; 7:689. [PubMed: 21460635]
35. McAlpine F, Williamson LE, Tooze SA, Chan EYW. Regulation of nutrient-sensitive autophagy by uncoordinated 51-like kinases 1 and 2. Autophagy. 2014; 9:361–373. [PubMed: 23291478]
36. Fleming TJ, Fleming ML, Malek TR. Selective expression of Ly-6G on myeloid lineage cells in mouse bone marrow. RB6-8C5 mAb to granulocyte-differentiation antigen (Gr-1) detects members of the Ly-6 family. J Immunol. 1993; 151:2399–2408. [PubMed: 8360469]

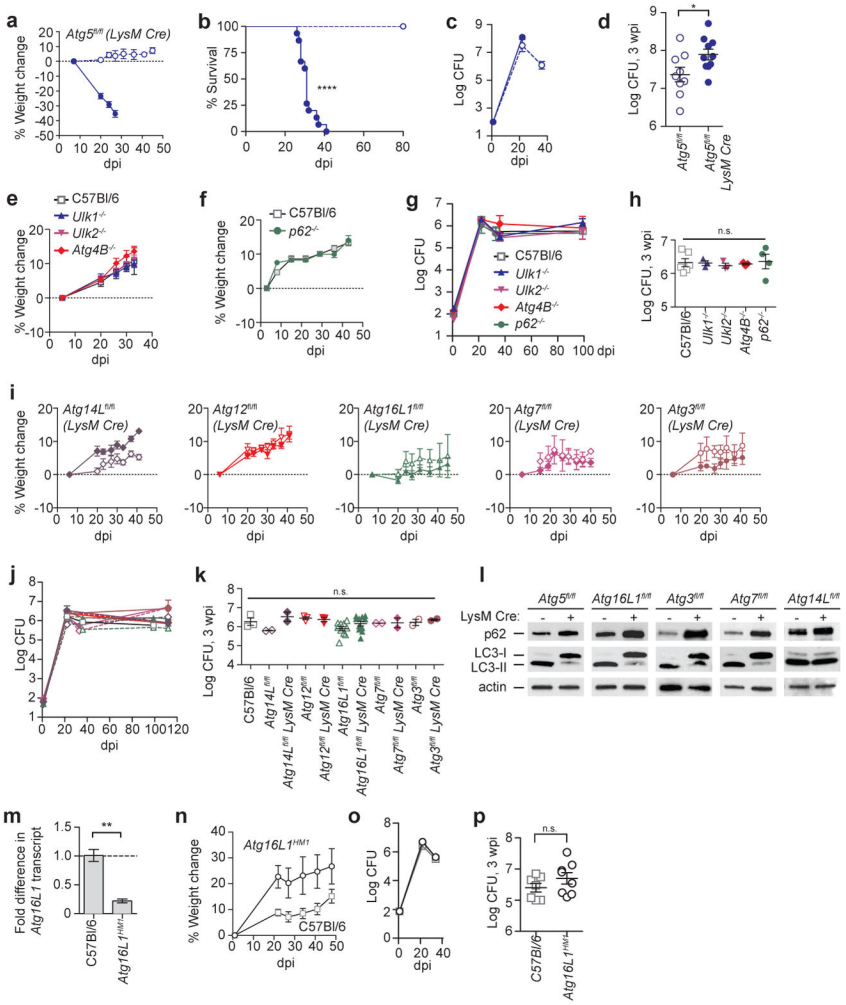

Figure 1. ATG5, in contrast to other ATG factors, is essential to control *Mtb* infection

a – k, Mice infected with approximately 100 CFU of *Mtb* were monitored at various days post infection (dpi) or weeks post infection (wpi). **a,** Weight change, **b,** survival, and **c, d,** log pulmonary CFU of $Atg5^{fl/fl}$ (open circles) and $Atg5^{fl/fl}$*-LysM-Cre* (closed circles). **e, f,** Weight change, and **g, h,** log pulmonary CFU of C57Bl/6 (open squares), $Ulk1^{-/-}$ (blue triangles), $Ulk2^{-/-}$ (inverted pink triangles), $Atg4B^{-/-}$ (red diamonds), and $p62^{-/-}$ (green circles) mice. **i**, Weight change and **j, k,** log pulmonary CFU of $Atg14L^{fl/fl}$*-LysM-Cre* (purple diamonds), $Atg12^{fl/fl}$*-LysM-Cre* (red inverted triangles), $Atg16L1^{fl/fl}$*-LysM-Cre* (green triangles), $Atg7^{fl/fl}$*-LysM-Cre* (pink diamonds), $Atg3^{fl/fl}$*-LysM-Cre* (brown circles) and corresponding floxed control mice. Floxed control mice are shown in open shapes, LysM-Cre-expressing mice are shown in closed shapes. **l,** Western blot analysis of p62, LC3 and actin in *ex vivo* peritoneal MΦ from uninfected mice. **m,** Fold change in *Atg16L1* transcript from $Atg16L1^{HM1}$ lungs as compared to C57Bl/6 at 3 wpi. **n,** Weight change and **o, p,** log pulmonary CFU of $Atg16L1^{HM1}$ (open circles) and C57Bl/6 mice (open squares). When used, center values represent the mean ± SEM. Statistical differences were determined by log-rank Mantel-Cox test (**b**), Student's t-test (**d, m,** and **p**) or one-way ANOVA and Bonferonni's multiple comparison test (**h, k**). * P < 0.05, ** P < 0.01, ****P < 0.0001.

Notable comparisons that were not significantly different are designated as n.s. Samples represent biological replicates. See Supplementary Fig. 1 for gel source data, Supplementary Fig. 2 for sample sizes and results from all statistical comparisons.

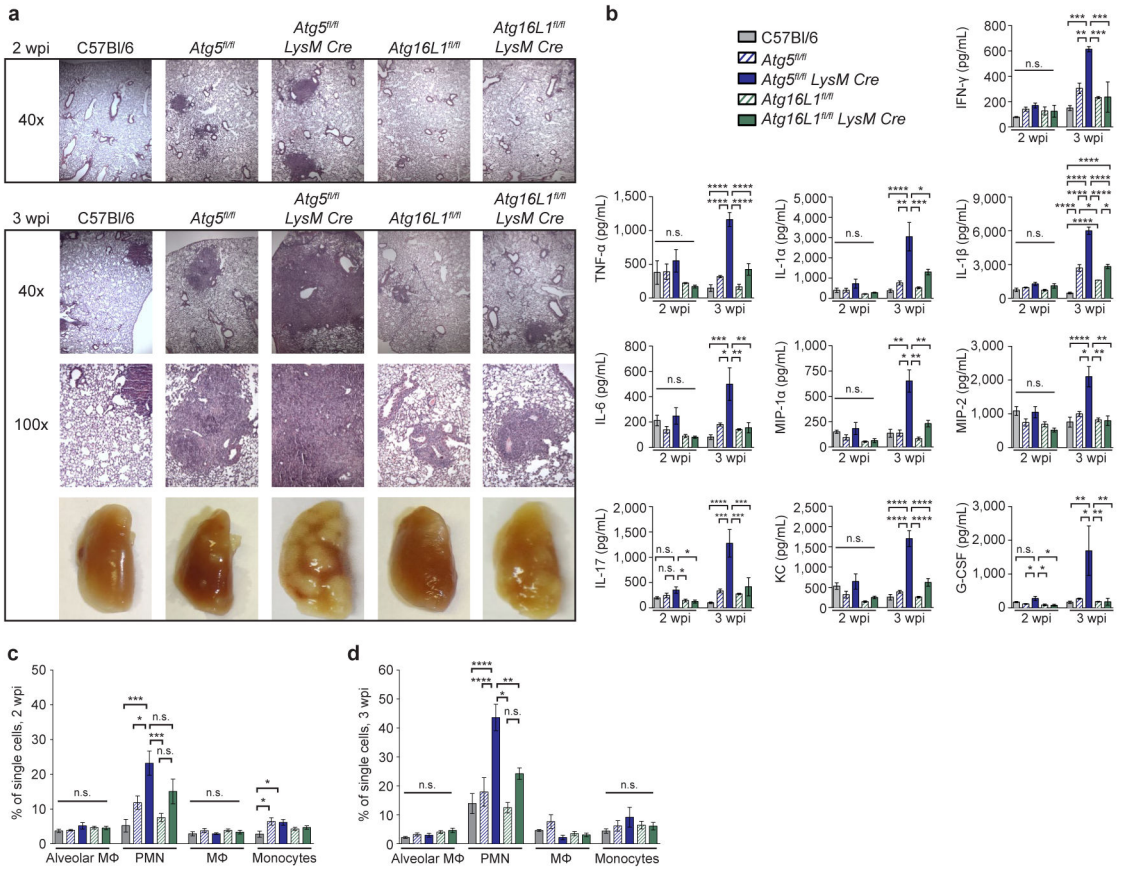

Figure 2. Loss of *Atg5* in LysM^{+} cells leads to earlier and more severe lung inflammation during *Mtb* infection

a, H&E stained histology of lungs at 2 and 3 wpi and gross pathology of lungs at 3 wpi. **b – d,** C57Bl/6 (grey solid bars), *Atg5$^{fl/fl}$* (blue striped bars), *Atg5$^{fl/fl}$-LysM-Cre* (blue solid bars), *Atg16L1$^{fl/fl}$* (green striped bars), *Atg16L1$^{fl/fl}$-LysM-Cre* (green solid bars). **b,** Concentration of cytokines in lungs (homogenized in 5mL) at 2 and 3 wpi as detected by ELISA. **c, d,** Frequency of alveolar MΦ, PMN, recruited MΦ, and inflammatory monocytes as a percentage of all single cells in lungs at 2 wpi (**c**) and 3 wpi (**d**). Statistical differences were determined by one-way ANOVA and Bonferonni's multiple comparison test (**b–d**). * $P < 0.05$, ** $P < 0.01$, *** $P < 0.001$, **** $P < 0.0001$. Notable comparisons that were not significantly different are designated as n.s. Samples represent biological replicates. See Supplementary Figure 2 for sample sizes and results from all statistical comparisons, Extended Data Fig. 5 for cytokine levels in uninfected lungs, and Extended Data Fig. 6 for gating strategy and number of cells in lungs.

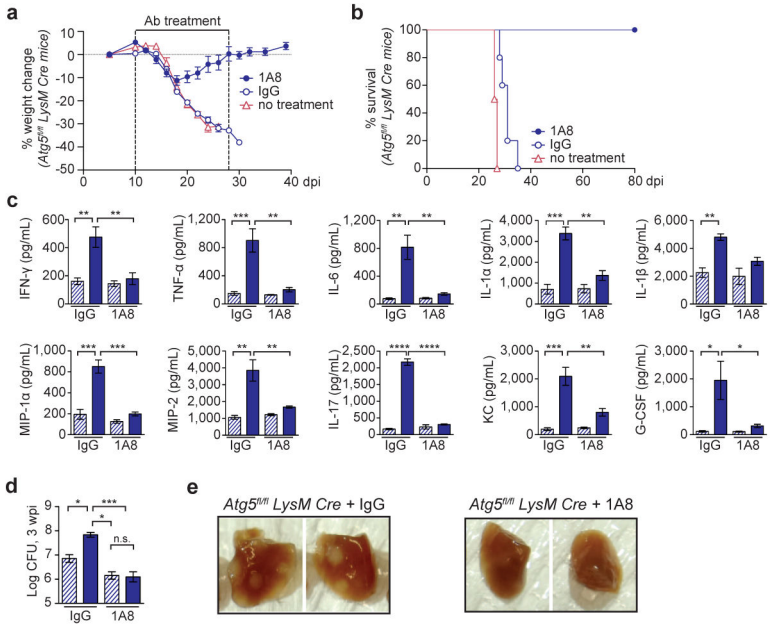

Figure 3. Depletion of PMN allows for survival of *Atg5*$^{fl/fl}$*-LysM-Cre* mice during *Mtb* infection

a, Weight change and **b,** survival of *Atg5*$^{fl/fl}$*-LysM-Cre* mice that received PMN-depleting anti-Ly6G (1A8, closed blue circle), isotype control (IgG, open blue circle), or no treatment (open pink triangle) every other day from 10 – 28 dpi. **c, d,** *Atg5*$^{fl/fl}$ (blue striped bars) and *Atg5*$^{fl/fl}$*-LysM-Cre* (blue solid bars) mice were treated with IgG or 1A8 and analyzed at 3 wpi. **c,** Cytokine concentration in lungs (homogenized in 5mL) and **d,** log pulmonary CFU. **e,** Pulmonary pathology of *Atg5*$^{fl/fl}$*-LysM-Cre* mice at 3 wpi following treatment with IgG or 1A8. Statistical differences were determined by one-way ANOVA and Bonferonni's multiple comparison test (**c, d**). * $P < 0.05$, ** $P < 0.01$, *** $P < 0.001$, **** $P < 0.0001$. Notable comparisons that were not significantly different are designated as n.s. Samples represent biological replicates. See Supplementary Figure 2 for sample sizes and results from all statistical comparisons.

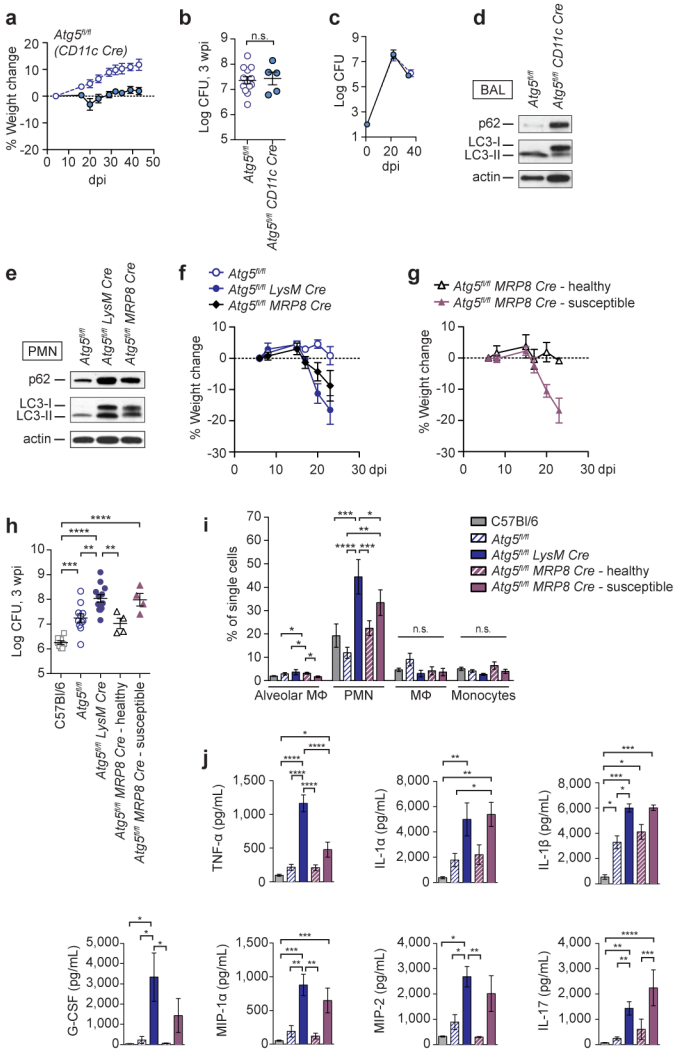

Figure 4. Loss of *Atg5* in PMN, but not alveolar MΦ or DCs, can cause susceptibility to *Mtb*

a, Weight change and **b, c,** log pulmonary CFU of *Atg5*$^{fl/fl}$ (open circles) and *Atg5*$^{fl/fl}$-*CD11c-Cre* (closed circles). **d,** Western blot analysis of p62, LC3, and actin in bronchoalveolar MΦ from *Atg5*$^{fl/fl}$ and *Atg5*$^{fl/fl}$-*CD11c-Cre* mice. **e,** Western blot analysis of p62, LC3, and actin in bone marrow PMN from *Atg5*$^{fl/fl}$, *Atg5*$^{fl/fl}$-*LysM-Cre* and *Atg5*$^{fl/fl}$-*MRP8-Cre* mice. **f,** Weight change of *Atg5*$^{fl/fl}$ (open blue circles), *Atg5*$^{fl/fl}$-*LysM-Cre* (closed blue circles), *Atg5*$^{fl/fl}$-*MRP8-Cre* (closed black diamonds) mice following infection with *Mtb*. **g,** Weight change of mice following infection with *Mtb*. 50% of *Atg5*$^{fl/fl}$-*MRP8-Cre* mice lost over 5% of their weight by 20 dpi ("susceptible," closed purple triangles) while 50% of *Atg5*$^{fl/fl}$-*MRP8-Cre* mice did not ("healthy," open black triangles). **h**, Log pulmonary CFU at 3 wpi. **i, j,** C57Bl/6 (grey solid bars), *Atg5*$^{fl/fl}$ (blue striped bars), *Atg5*$^{fl/fl}$-*LysM-Cre* (blue solid bars), "healthy" *Atg5*$^{fl/fl}$-*MRP8-Cre* (purple striped bars), and "susceptible" *Atg5*$^{fl/fl}$-*MRP8-Cre* (purple solid bars). **i,** Concentration of cytokines in lungs (homogenized in 5mL) at 3 wpi. **j,** Frequency of alveolar MΦ, PMN, recruited MΦ, and inflammatory monocytes as a percentage of single cells in lungs at 3 wpi. When used, center values represent the mean ± SEM. Statistical differences were determined

by one-way ANOVA and Bonferonni's multiple comparison test (**h–j**). * $P < 0.05$, ** $P < 0.01$, *** $P < 0.001$, **** $P < 0.0001$. Notable comparisons that were not significantly different are designated as n.s. Samples represent biological replicates. See Supplementary Figure 2 for sample sizes and results from all statistical comparisons, and Extended Data Fig. 7 for total numbers of cells in lungs.